Aerodynamic Studies of High Advance Ratio Rotor Systems

Todd R. Quackenbush, Daniel A. Wachspress,
Robert M. McKillip, Jr., and Marc J. Sibilia
Continuum Dynamics, Inc.
todd@continuum-dynamics.com

ABSTRACT

This paper describes ongoing experimental and computational work motivated by increasing interest in high speed rotorcraft. While the long term goal of this activity is to develop improved computational models for high advance ratio rotary wing aerodynamics, a key aspect of work to date has been wind tunnel testing of a simple rotor system at very high μ. These tests have been designed to provide data on rotor performance both guide model development and expand the available validation database for high advance ratios. Key results of recent test entries are described including of rotor lift and drag for advance ratios above 2.0, as well as development of H force data for these conditions. In addition, flow visualization studies using tufted blades were conducted that provided insight into local on-blade flows. Limited validation studies with newly enhanced rotor analysis tools are presented. Finally, goals are outlined for follow-on testing that will address remaining open issues

NOMENCLATURE

a_{1s}	longitudinal flap angle, deg
b_{1s}	lateral flap angle, deg
c_{do}	minimum profile drag coefficient
c	rotor blade chord length, ft
C_L	rotor lift coefficient, $L/(0.5\rho U^2 S)$
C_T	thrust coefficient, $T/\rho\pi R^2(\Omega R^2)$
c_d	drag coefficient, $d/(0.5\rho U^2 c)$
C_H	horizontal force coeff., $H/\rho\pi R^2(\Omega R)^2$
C_Q	profile torque coeff., $Q/\rho\pi R^3(\Omega R)^2$
H	rotor horizontal force, lbs.
L	rotor lift force, lbs.
N_b	number of blades
R	rotor radius, ft
V	free stream speed, fps
α_s	rotor shaft angle of attack, rad
α_{TPP}	tip path plane angle of attack, rad
ρ	air density, slug/ft^3
σ	rotor solidity, $N_b c/\pi R$
μ	advance ratio $V/\Omega R$
ψ	rotor azimuth angle, deg

INTRODUCTION

Current investigations of high advance ratio vehicle concepts have rekindled interest in a wide range of rotor aeromechanical analysis and design issues encountered in several past studies of gyrocopters and high speed rotor systems ([1]-[5]). Recent studies of modern gyrocopters, slowed rotor compounds, and advancing blade concepts (e.g., [6]-[9]; see Figure 1) have helped revive interest in this topic but have also made clear both the many limitations of current models in analyzing the high μ regime and the scarcity of relevant data.

Presented at the 67th Annual Forum of the American Helicopter Society, May 2-4, 2011, Virginia Beach, VA.

This paper will describe key results of an investigation of various aspects of high μ aerodynamics that included a series of rotor tests along with enhancements to existing analytical and computational models. This multi-track effort included: 1) wind tunnel tests of a model rotor at advance ratios up to and above 2.0; 2) analytical enhancements for comprehensive rotorcraft analyses to improve modeling of rotor performance in highly yawed and fully reversed flow; and 3) analysis of airfoil sections and rotor blades in high advance ratio flight using state of the art computational fluid dynamics analysis methods. The present paper focuses on the first two areas and extends the report of initial work in [10] and [11]; the status of complementary work on CFD analysis at high advance ratios was summarized in detail in [12] and has been further extended by a contemporary paper [13].

Figure 1: High speed rotorcraft concepts (left to right): Sikorsky X2; Carter Aviation demonstrator; GBA/ DARPA Heliplane military and civil concepts.

EXPERIMENTAL SETUP

The test apparatus employed in this project included the articulated rotor test rig shown in Figure 2. Earlier variants of this rig were used to produce results described in [10] and [11], which included rotor lift and drag measurements on high advance ratio rotors. The

goal of testing activity to date has been was to obtain rotor performance and blade motion data for a broad range of operating conditions at high μ. Ideally, our goal was to address advance ratios as high as 2.5 to allow analysis of a wide range of novel conceptual vehicles. As will be seen, the experiments conducted here were able to approach but not yet reach this plateau, though follow-on testing described at the end of the paper may be able achieve this goal.

While in general it is desirable to have results for both powered and autorotating rotors, tests to date have focused on the latter case; such cases are of considerable interest for slowed rotor compound vehicles, such as the ongoing DARPA-sponsored Heliplane development [14]. Such results are also readily compared to prior investigations of gyrocopters (e.g., [1] and [5]).

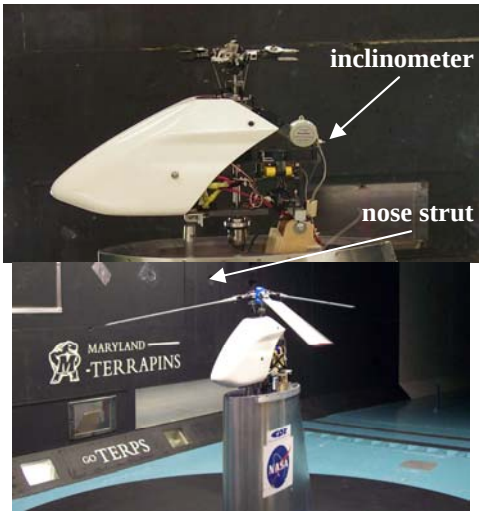

Figure 2: (Above) side view of the installed test stand with the airframe at zero deg. shaft angle of attack, and (below) oblique view of the model with blades installed.

The test venue for our experiments was the Glenn L. Martin Wind Tunnel at the University of Maryland. The test apparatus was developed by modifying readily acquired rotor and drive system hardware from a radio controlled helicopter. While this limited the loads and test conditions achievable, as will be seen results obtained with this apparatus compared well with prior full scale tests. The rotor configuration involved three blades with hinged root attachment and yielded a rotor, 52" in diameter. The blade set used is shown in Figure 3a; the blades measure 23.64" (600 mm) long, have a 2.24" (57 mm) chord with zero built in twist and a 0.12 thickness to chord ratio. The blade sections were found to very closely approximate a NACA 0012 profile.

Figure 3b shows a schematic of the test stand, along with the fairing used to minimize loads on support struts. The fairing itself was non-metric, and the test plan included measurement of the tare loads of the support stand (wind on and wind off) for use in the data reduction process. The testing focused on measurements of RPM and blade flapping, in particular to measure the autorotative RPM for a range of collective, cyclic and shaft angle settings; lift and drag was measured using the tunnel balance.

Figure 2 shows two views of the installed model; Figure 2a shows the model (with no blades mounted) at a shaft angle of attack of zero; an electrically actuated nose strut allowed angle adjustments during the test, and an inclinometer on the model provided shaft angle of attack data. Figure 2b shows the positioning of the rotor in the tunnel with blades installed. As indicated in Figure 3, the test rig was connected to the tunnel balance to permit the measurement of forces and moments during the test.

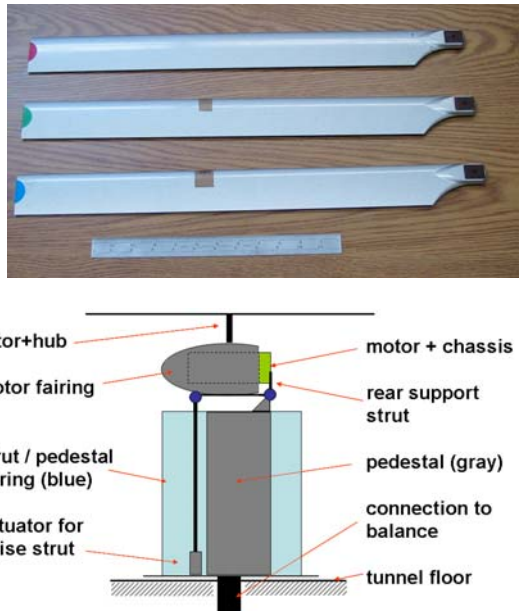

Figure 3: a) above - rotor blade set used in wind tunnel experiments. b) below – schematic of the test stand, fairing, and interface to the tunnel balance, approximately to scale (side view).

For recent test entries, the test stand was modified with load cells to provide an interim torque measurement capability, as well as a consistency check on tunnel balance drag measurements. Modifications were made to install two load cells laterally offset from the stand centerline, as shown in Figure 4. The upper chassis was mounted on flexures to isolate the load paths and permit streamwise (drag) loads to be reacted through the load cells; differential loads would reflect torque on the model. A calibration matrix was generated in pre-entry lab tests to translate measured voltages to drag force and torque. (Note: as discussed later, follow-on tests are planned with a direct rotor torque sensor in place).

To set up autorotation a given tunnel speed, a shaft angle of attack was selected, along with initial collective and cyclic pitch settings (root pitch control inputs were controllable during a run, but were typically fixed during most of the duration of a test). A DC power supply controlling the electric motor was used to increase RPM to a level above that expected for autorotation; "flying" the rotor in these shakedown tests was done carefully at first to balance the imperatives of preventing a rotor overspeed and not allowing RPM to decay to the point where excessively high advance ratio could lead to high rotor vibration and/or possible instabilities. The most convenient method for controlling rotor RPM involved decreasing electrical power input to the drive motor until steady RPM was achieved with zero voltage, indicating the tunnel flow was driving the rotor. With such an initial autorotative state established, the shaft angle of

attack was gradually reduced (typically in increments of 0.2 to 0.5 deg.) and rotor RPM recorded. This approach allowed a wide range of advance ratios to be achieved.

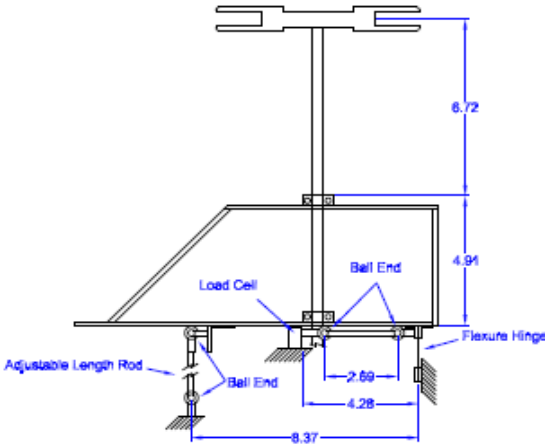

Figure 4: Schematic of side view of the modified chassis showing load cell installation locations.

Along with tunnel speed, the key measurements recorded included shaft angle of attack α_s (using the inclinometer shown in Figure 2) and rotor blade flap and pitch angles (via Hall effect sensors at the blade root). Integrated forces on the test stand were measured with the wind tunnel balance. Pre-test wind-off and wind-on tares (both with and without rotor blades) were measured to remove the stand effects on rotor force measurements. Since rotor drag was of particular interest (see the discussion below) careful pre-test calibrations were conducted that established the precision of the balance in the drag axis to be < 0.3 oz. (~9 gms.).

RECENT TEST RESULTS

The test points detailed below were selected to build on the results of prior testing; selected results from these tests are now briefly summarized to provide background for further discussion. Figure 5 shows a representative set of results from [10], capturing measured lift and drag on the rotor at advance ratios up to 1.7 in autorotation. Comparison to data taken on the 3-bladed PCA-2 autogyro [1] shows the considerable overlap with this pre-existing data. This favorable comparison indicated the utility of this relatively simple rotor test apparatus in capturing useful rotor data.

In the July 2009 tests, the first four runs entailed reacquisition of tare data – given changes owing to the introduction of the load cells since the prior entry – while Runs 5 and 6 involved new force measurement data. In these two runs, it was possible to directly compare balance data with measurements from the strain gauge load cells depicted in Figure 4. Figure 6 shows the comparison of tunnel balance and strain gauge load cell data from Run 5 for rotor drag, which is a particularly sensitive measurement. Figure 6 shows the close agreement between these two separate measurements.

Full lift and drag coefficient data for two autorotation runs up to and beyond advance ratio 2.0 are shown in Figure 7 and 8. As is evident, the qualitative trends are similar to those reported in Ref. 11 from the April 2009 test, though the introduction of cyclic pitch at approximately $\mu = 1.6$ – to prevent excessive flap motion - produces a change in slope of the force coefficient trends with increasing advance ratio.

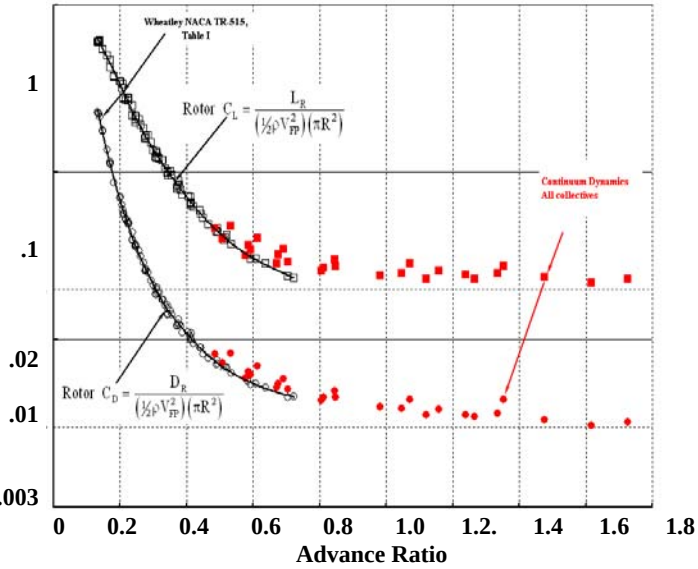

Figure 5: Measured rotor lift and drag coefficients for the model rotor (all collective settings for multiple test runs and 90-110 fps tunnel speeds) compared to PCA-2 wind tunnel data from [1] (figure from [10]).

Ref. [11] discusses initial tests executed in April 2009 that reached still higher advance ratios approaching and in some cases exceeding 2.0. Additional test runs executed in July 2009 also exceeded this level and afforded the opportunity to confirm previously observed results in terms of rotor drag force. As noted above, final rotor lift and drag coefficient plots for individual cases were produced by subtracting out the wind-on tare measurements from the balance data, using specific tares developed for each combination of tunnel speed and shaft angle of attack.

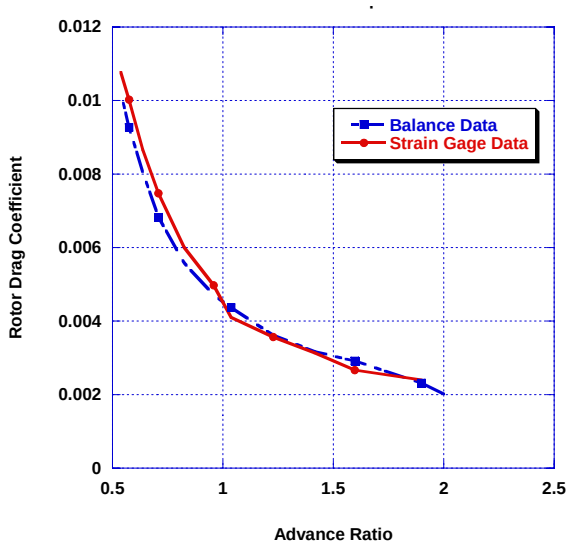

Figure 6: Run 5 drag coefficient measurements: strain gage vs. balance data.

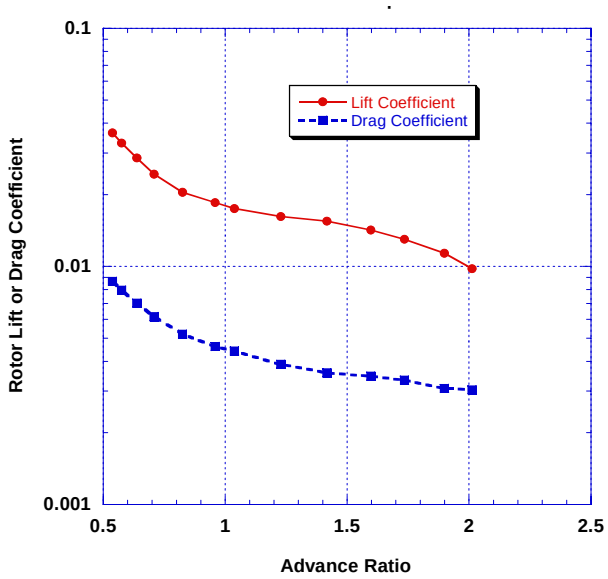

Figure 7: Rotor lift and drag coefficient vs. advance ratio at 110 fps., and 0 deg. collective; lateral cyclic introduced at μ = ~1.6.

It was observed during Runs 5 and 6 that the collective pitch of the blades changed during the run as RPM dropped, moving from an initial setting of 0 to approximately -1 deg. as RPM was reduced from approximately 1000 to 300. Second, above roughly advance ratio 1.2, a considerable blade to blade divergence appeared in the flap motion and grew with increasing advance ratio, leading to several degrees difference in measured flap response for each blade.

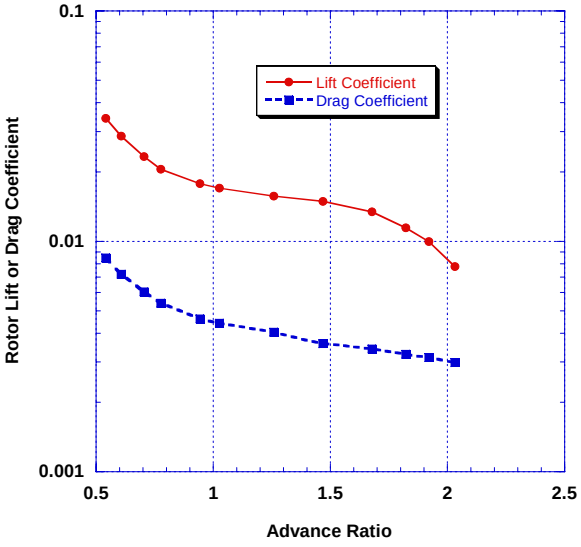

Figure 8: Rotor lift and drag coefficient vs. advance ratio at 115 fps. tunnel speed and 0 deg. initial collective; lateral cyclic introduced at ~μ = 1.6.

At the time of the test, it was postulated that coarseness of available settings on rotor pitch links contributed to this phenomenon, in that it was difficult to make a precise blade-to-blade match in root pitch control, which in turn affected the ability to closely control blade tracking; one of the test stand modifications put in place for the projected final test entry – pitch links with a fine adjustment capability - addresses this point. For the purposes of analyzing mean rotor drag below, average values of rotor longitudinal flap and collective pitch were computed (Figure 9).

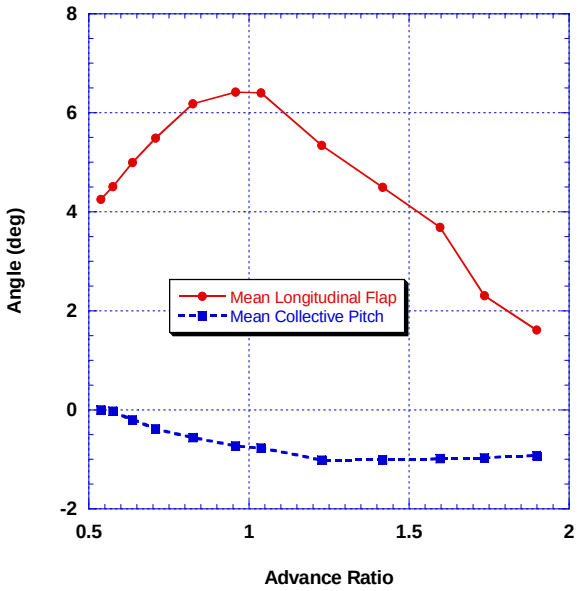

Figure 9: Rotor mean longitudinal flap angle and collective pitch at 110 fps. tunnel speed (Run 5).

This result was used to further explore the computation of rotor in-plane force from this data set, an issue first addressed in [11]. The tip path plane angle for these runs was determined using $\alpha_{TPP} = \alpha_s + a_{1s}$ (using the mean a_{1s} values in Figure 9). The component of rotor drag coefficient owing to the action of rotor thrust for a given tip path plane orientation can be approximated here as $C_L\alpha_{TPP}$, and the quantity $C_D - C_L\,\alpha_{TPP}$ is plotted in Figure 10 for Runs 5 and 6. The rotor in-plane force coefficient can then be computed for these same runs, using

$$C_H = (C_D - C_L\,\alpha_{TPP})\,(\mu^2/2) \qquad (1)$$

As is seen in Figure 11, the results were quite consistent for both Runs 5 and 6.

It was of interest to compare the measured results to analytical approximations. One such comparison involved plotting measured C_H against an approximation to high $\mu\,C_H$ (drawn from [15]) for rotors with zero shaft angle of attack and zero collective pitch. (Note: here a c_{d0} value of .01 was initially assumed for this small scale NACA 0012 section).

$$C_{H0} = (\sigma c_{d0}/8)(3\mu + 1.98\,\mu^{3.7}) \qquad (2)$$

Figure 11 also shows this prediction compared to the experimental results. While clearly direct comparability is not expected, the fact that the result for the lift-carrying experimental rotor predicts higher C_H than the nonlifting, zero-collective theoretical curve is reasonable. However, this comparison was made without direct information on the actual drag characteristics of the rotor; additional measurements were made in subsequent experiments (described below) that made this possible.

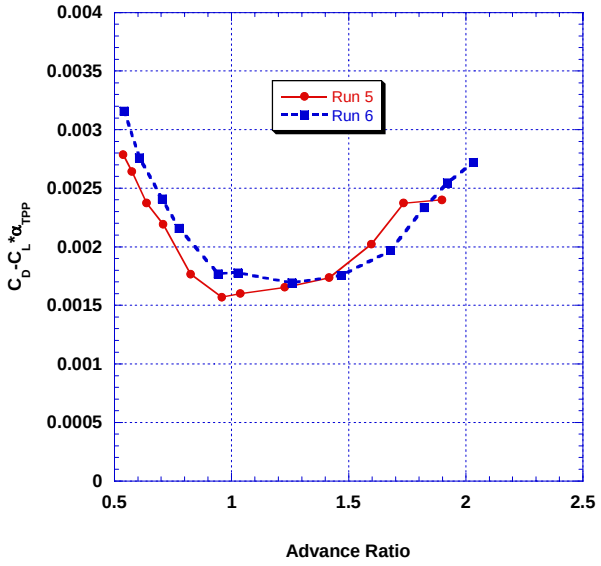

Figure 9: Net rotor drag coefficient, adjusted to remove rotor lift coefficient component in the streamwise direction; results shown for Runs 5 and 6.

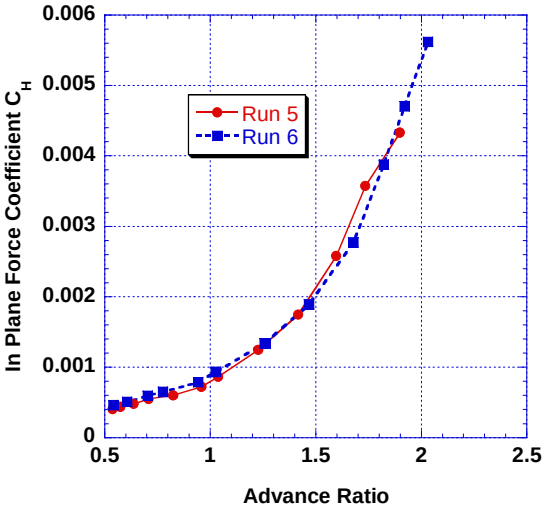

Figure 10: Measured rotor in-plane force coefficient shown for Runs 5 and 6.

FLOW VISUALIZATION RESULTS

Another feature of recent tests has been flow visualization through the use of surface mounted tufts. The outboard region of one blade was tufted and overhead camera and flash system (see Figures 12 and 13) was used to gather qualitative data on flow behavior at very high μ. Ref. [11] includes a series of photos covering cases at increasing advance ratio; here we focus on a more detailed study of two high μ cases.

The operating condition shown involved the wind tunnel rotor at advance ratio 1.7. The rotor was operating at this point at an RPM of 280 with a tunnel speed of 110 fps. Rotor shaft angle of attack was 2.8 deg. and lift coefficient was 0.016. Rotor collective input during this test point was -1.1 deg., while zero cyclic pitch was employed. The camera positioning and field of view was such that a nearly complete view of the entire rotor disk could be obtained with a single shot (Figure 14). (Note: this rotor features a clockwise rotation, opposite that of typical U.S. rotorcraft).

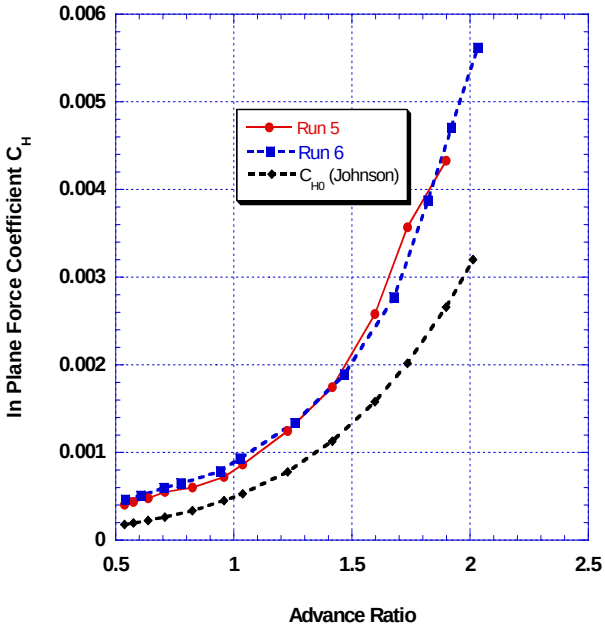

Figure 11: Comparison of experimental results for in-plane force for Runs 5 and 6, including an analytical prediction for zero collective and zero shaft angle.

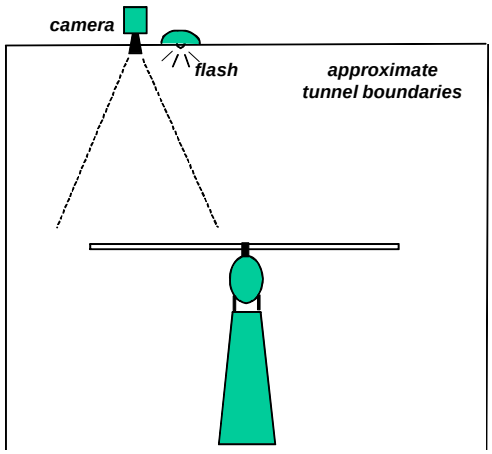

Figure 12: Schematic of wind tunnel layout, showing overhead camera system.

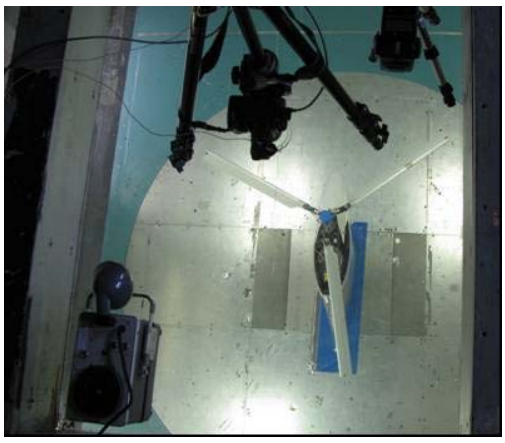

Figure 13: Overhead view of camera system.

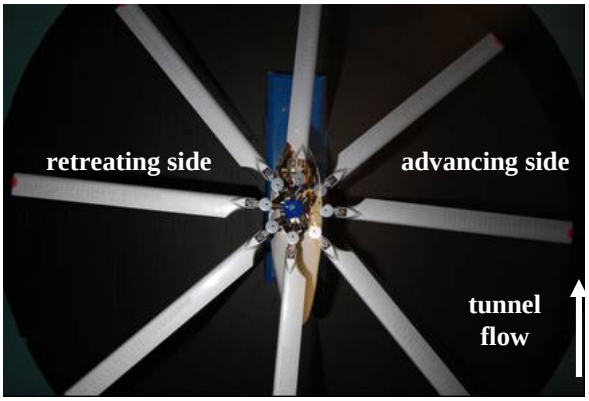

Figure 14: Overhead view of tufted rotor blades - composite showing all rotor azimuths at advance ratio 1.7.

The resolution of the photographs is such that closeups at particular azimuth locations can yield considerable detail on flow behavior. Figure 15 shows the flow at ψ = 276 deg., which indicates irregular regions of reverse flow across the tufted region. By the point the blade reaches ψ = 306 deg., strongly yawed flow has taken over, with the flow being nearly radial at several spanwise locations, though the apparent yaw angle decreases for outboard segments. Figure 16 shows a sequence of four views of the rotor as it traverses the advancing side of the disk; the tuft patterns reflect the shifting yawed flow behavior through this region. The tuft patterns at ψ = 39 and 141 indicate the (expected) very high yaw angles in the first and second quadrants.

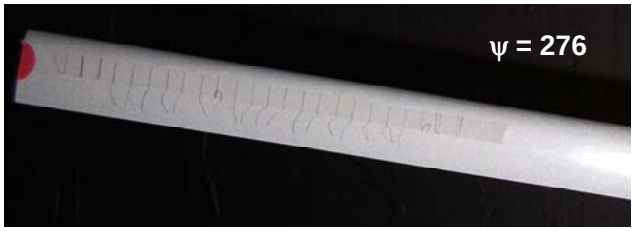

Figure 15: Closeup view of tufted rotor blade at azimuth angle 276 deg. at advance ratio 1.7.

More complex behavior becomes apparent at ψ=219 deg. Here, the tufts indicate mixed behavior suggesting differing directions of strongly radial flow. Given the kinematics of the onset flow shown in Figure 18, this flow pattern clearly indicates some unanticipated mechanisms at work. At this azimuthal location, the geometric trailing edge is the aerodynamic leading edge of the blade, and it is possible that flow separation from the sharp geometric trailing edge produces a strong vortical structure that accounts for the large observed deviation from the kinematic flow resulting from the rotational (Ωr) and onset (V) flow that dominates most of the other observed locations. As is seen in Figures 19 and 20, the flow at this azimuth location more closely follows the kinematic flow at advance ratio 1.0. Further studies of this region were made in the final test entry following modifications to the test stand.

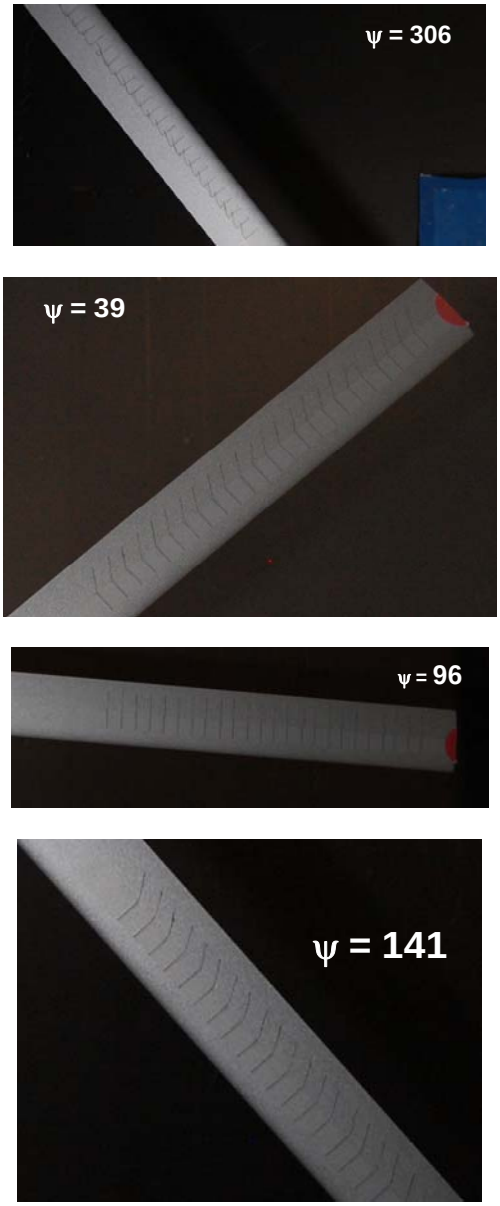

Figure 16: Closeup view of tufted rotor blade at four azimuth angles at advance ratio 1.7.

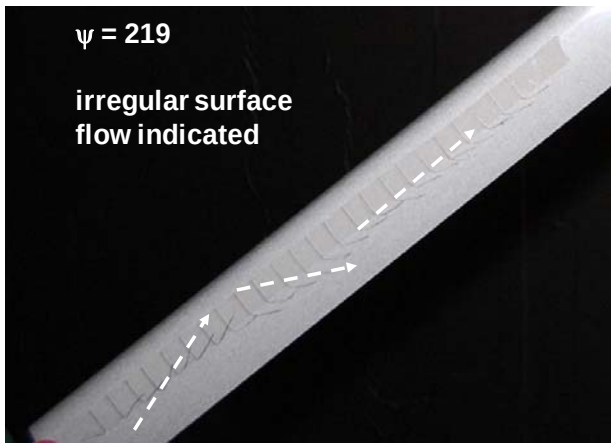

Figure 17: Closeup view of tufted rotor blade at azimuth angle ψ=219 at advance ratio 1.7.

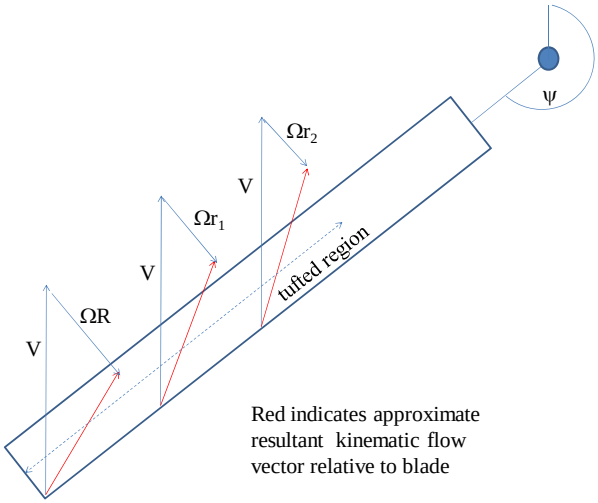

Figure 18: Schematic of kinematic flow components at azimuth angle ψ=219 for advance ratio 1.7.

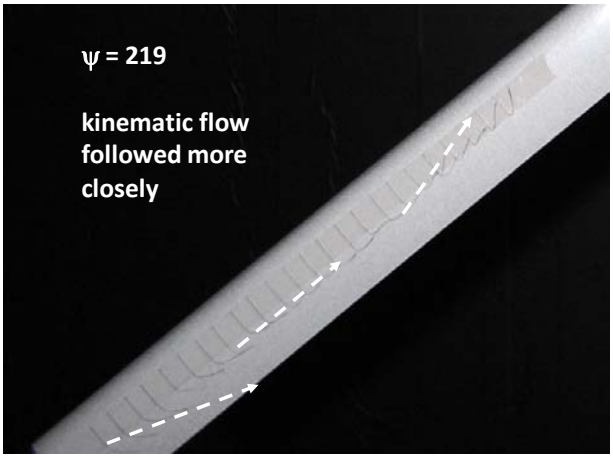

Figure 19: Closeup view of tufted rotor blade at azimuth angle ψ=219 at advance ratio 1.0.

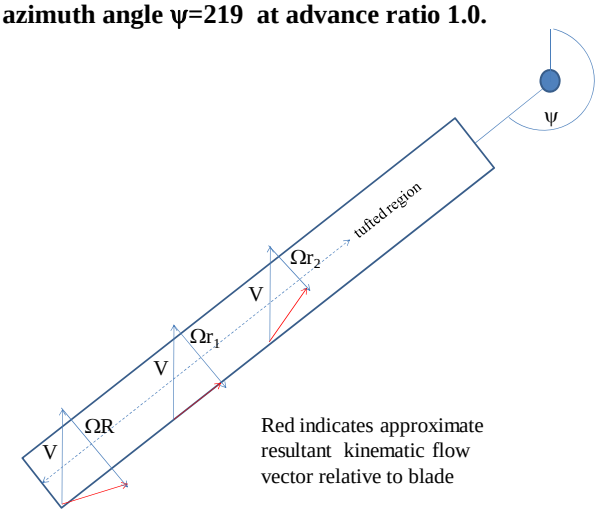

Figure 20: Schematic of kinematic flow components at azimuth angle ψ=219 for advance ratio 1.0.

Final Test Entry

The second entry in July 2009 included a mishap that significantly damaged the test stand. Over the succeeding months, a new, more robust design was developed, featuring a number of new elements:

- key elements of the model chassis were replaced and/or strengthened;
- the angle of attack actuator rod attachment was redesigned and slack removed from the actuator to mitigate fatiguing vibration;
- the footing attaching the test stand to the tunnel was stiffened to reduce stand motion;
- a new pedestal was designed comprised of welded steel, removing some flexibility introduced by the prior wooden pedestal;
- provision was made for easier blade tracking via fine threading on the pitch links; close blade tracking helped reduce large 1P loads.

Figure 21 shows the new test stand installed in the wind tunnel prior to the final tunnel entry.

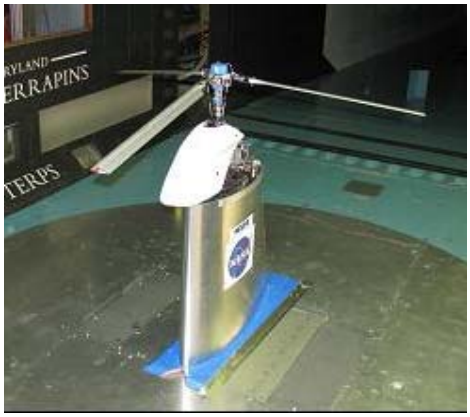

Figure 21: New rotor test stand with torque instrumentation installed.

Another major design change introduced in this test stand involved use of a torque sensor mounted in the rotating reference frame to permit data to be generated from powered runs. Figure 22 shows the rotor hub height extension that results from the addition of the in-line torque gauge on the shaft, which in turn required the use of extended pitch link arms to connect to the swashplate.

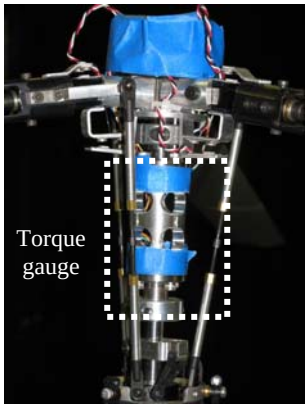

Figure 22: Closeup of torque sensor installation.

With the addition of the torque gauge, some additional modifications were required in the rotor model instrumentation package. Since the slipring assembly on the model only had eight available channels, it was decided to provide amplification to the

torque gauge in the rotating frame, using a small instrumentation amplifier IC. But even with that modification, the combined total of three blades having individual sensors for both flap and pitch angle meant that all of the sensor data and power channels could not be accommodated by the slipring. Instead, further modifications were made to provide a microcontroller to digitize these sensor signals at the rotor hub, and transmit a differential serial data stream from the model back to the control room.

Consequently, a specialized hub instrumentation card was designed and built to accomplish this task, and has the added benefit that it may communicate (again, through a secondary serial interface) with additional sensors coupled to associated microcontrollers. A circuit card mounted on the top of the hub incorporated a Microchip dsPIC33F series microcontroller, two differential serial transceivers, and an integrated differential amplifier chip for the torque measurement. Hall effect sensors were used to measure flap and pitch angles on the fully articulated hub assembly (Figure 23), and these signals are reduced through a resistor network and fed directly to the analog input pins on the dsPIC microcontroller. A 5-pin interface was provided for in-circuit reprogramming, allowing various sampling schemes and data processing features to be added as needed by the test program.

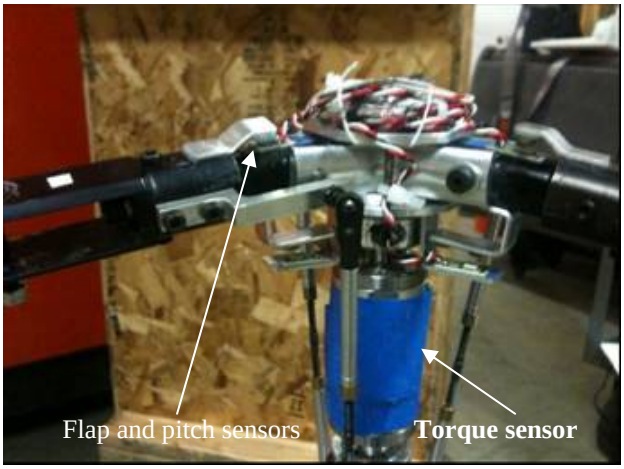

Figure 23: Rotor torque gauge installed onto the rotorl shaft (covered in blue tape) below hub.

Static calibration was conducted on the torque sensor (a Futek TFF325 device with maximum capacity 50 in-lb.) and the flap at pitch sensors. With these subsystems in place, shakedown testing in hover was conducted at CDI at rotor RPM levels up to 800. Functionality of the sensors was confirmed and sample data runs executed to confirm readiness for wind tunnel installation. However, one limitation that was observed was the occurrence of significant stand resonance at roughly 850 RPM. This resonance persisted despite alterations to the anchoring of the stand and other adjustments; thus, operating RPM for the projected test was limited to roughly 700 to ensure safe operation through this final test entry.

The modified rotor stand was put installed in the G.L. Martin wind tunnel, as indicated in Figure **21**. Along with additional wind-on and wind-off tare runs to measure the effect of the new rotor configuration, 20 data runs were executed over approximately two days of testing that provided additional data confirming earlier autorotation runs, extending the prior data gathering to include powered rotor cases, and adding to the available body of flow visualization results presented below.

The initial performance shakedown runs executed focused on hover runs with low collective pitch to both verify the operation of the torque sensor as well as to provide updated estimates of rotor drag. Figure 24 shows the measured results from a case with a nominal initial collective pitch of 0 deg. but at increasing RPM. (Note: the maintenance of near zero thrust was expected to minimize distortion of the results by recirculation in the closed test section). Here, both dimensional torque in in-lbs. is shown, along with an estimate for mean drag coefficient on the rotor, based on the assumption that $C_{q0} = \sigma c_{d0}/8$. As is evident, the measured torque increases monotonically, though it does not following the quadratic dependence of torque with RPM that might be expected at constant collective pitch. However, it was of interest that the estimate drag coefficient dropped as a function of RPM; it is possible that the increase in Reynolds number over the rotor span (from a chord Re of roughly 70,000 at 300 RPM to 165,000 at 700 RPM. These very low Re values can produce mean zero-lift drag coefficients that are well above the levels of .008-.012 expected for high Re airfoils.

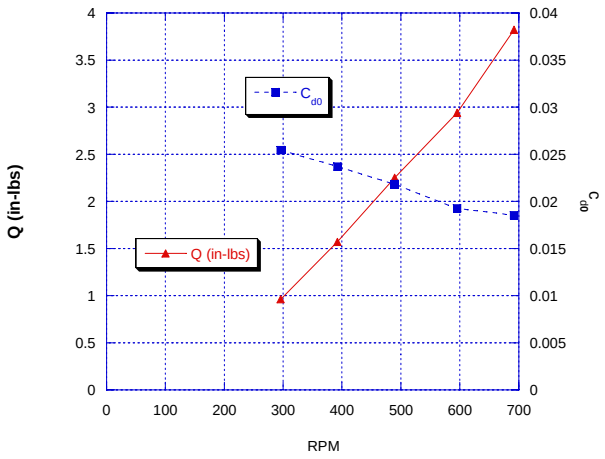

Figure 24: Torque and effective zero lift drag coefficient for the model rotor in hover; RPM sweep at fixed collective.

One byproduct of this measurement was an interest in revisiting Figure 11, which compared a simple analytical model of rotor in plane force to the measured data from prior runs. This analytical model assumed a mean rotor drag coefficient of .012. If this is increased to a mean level of .02 (using the measurements shown in Figure 24) the revised comparison shown in Figure 25 is obtained. This increase in mean drag coefficient can provisionally be assumed to be due to low Re effects on rotor drag, but clearly additional analysis is necessary to confirm this. However, should this assumption prove correct, it may be that the high μ measurements of in plane force made for the cases discussed above can be captured with relatively simple models.

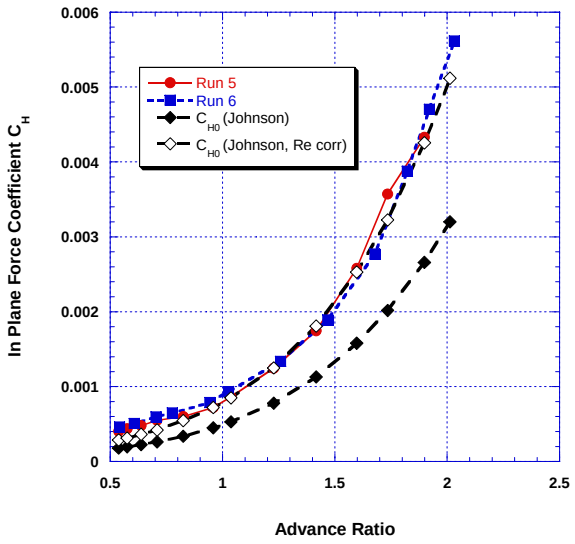

Figure 25: Revised version of Figure 11, comparing measured in-plane force coefficient (Runs 5 and 6 of the second wind tunnel entry) to the theory of Eqn. 2, using an increased mean drag coefficient derived from experiment.

Following these initial runs, experiments were undertaken at low tunnel speed (60 fps) and in autorotation to ensure that rotor performance points (in terms of autorotation envelopes of RPM vs. shaft angle of attack for a fixed tunnel speed) obtained in earlier testing could be recovered. Additional runs were then executed examining the performance of rotors in powered operation at high advance ratio. These were undertaken by setting up the rotor at moderate advance ratio and an operating condition representative of propulsive flight and then gradually reducing RPM at a fixed tunnel speed.

Figure 26 shows the envelope of rotor lift and drag coefficients vs. advance ratio obtained for two runs in which tunnel speed was held constant at 60 fps and RPM was dropped from a starting value of 700 to final values in the 260-280 range, the run being limited by the desire to keep flap amplitude (which was measured separately) from exceeding +/-6 deg. In these cases, shaft angle of attack was -4 deg. and rotor collective pitch was fixed at +3 deg. with zero cyclic pitch. As is evident, there is some scatter in the measurements, but they provide a wide range of lift and advance ratio values. Measurements of rotor torque coefficient for these cases are shown in Figure 27. Again, moderate scatter is observed but the measured data provides a reasonable range of conditions for correlations studies with the methods discussed below

COMPUTATIONAL MODELING RESULTS

Work on this project also featured analytical activity that focused on development of improved yawed-flow corrections for lifting line and lifting surface theories for use in high speed flight. Implementation was focused on an existing lifting surface/full-span, free-vortex wake model – the Constant Vorticity Contour (CVC) representation in the CHARM software [16]. This analysis was extended using a "Generalized CVC" or GCVC model to support wake release from the "leading edge" of the blade in reverse flow. Figure 28 shows an example for an H-34 main rotor modeled on that tested in [4].

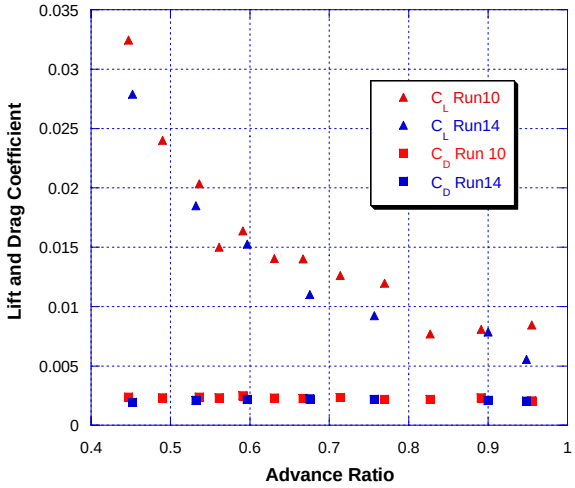

Figure 26: Rotor lift and drag coefficient at fixed tunnel speed; RPM sweep at fixed collective of +3 deg. and fixed shaft angle of -4 deg (Runs 10 and 14).

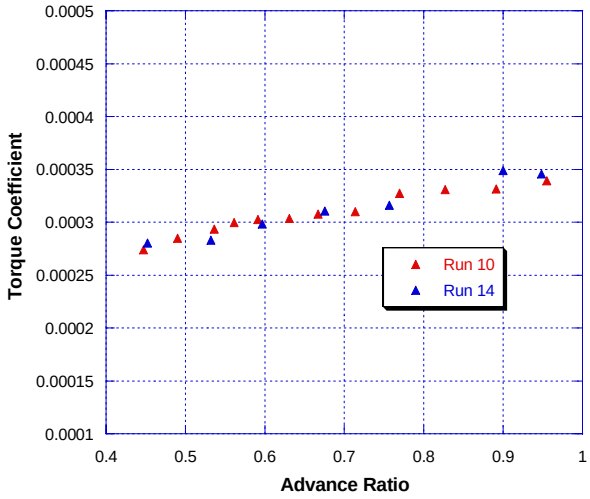

Figure 27: Rotor torque coefficient at fixed tunnel speed; RPM sweep at fixed collective of +3 deg. and fixed shaft angle of -4 deg (Runs 10 and 14).

Along with improvements in yawed flow and near field wake modeling, a critical upgrade to CHARM capabilities for high advance ratio cases has been the addition of airfoil data tables for sections operating in strongly yawed and reversed flow. These tables were generated by OVERFLOW, using methods introduced by Smith et al. [12]. Earlier correlation studies with the H-34 rotor using the upgraded CHARM model were reported in [11]. Our validation work has also included comparison with a reduced-diameter UH-1 rotor at high advance ratio, tests of which were described in [17].

As detailed in [17], the diameter of this two bladed set was reduced from 44 ft. for the standard UH-1 to 34 ft. This variant also featured a low (-1.42 deg.) blade

twist level and an atypical built-up inboard section with doublers attached to reinforce the blade/hub attachment; details of this geometry are discussed in [8]. A NACA 0012 section was used for the lifting components of the rotor system; the doublers used for root reinforcement tapered to the 0012 section outboard of 0.39R. Tests of the rotor were conducted at advance ratios from 0.51 to 0.75, offering a useful data set for correlation of the revised CHARM model.

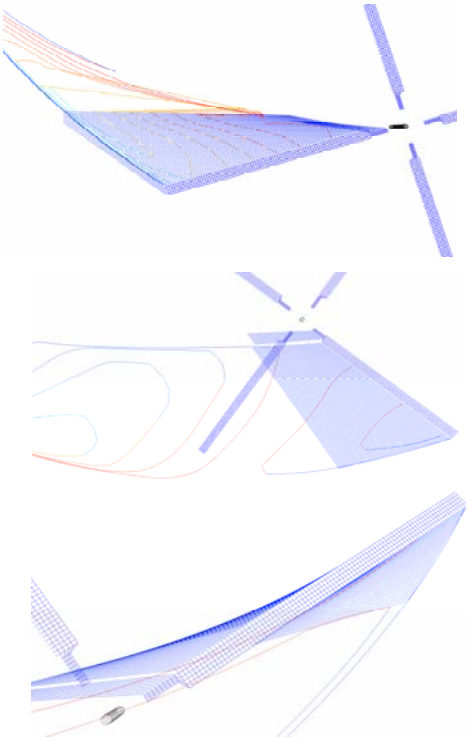

Figure 28: Three snapshots of Generalized CVC (GCVC) wake filaments and near field trailers for a four-bladed H-34 rotor at advance ratio 1.0.

A first objective was to compare the slope of rotor lift vs. shaft angle of attack for zero collective pitch (at 0.75R). As seen in Figure 29, CHARM yields qualitatively good results in predicted thrust at zero collective, but with an offset of .003-.005 in lift coefficient at advance ratio 0.51. Predictions of lift coefficient for advance ratio 0.75 produced considerably more irregular results, with significant deviations from measured lift at shaft angles 4 and 8 deg. (Figure 30); investigation of these cases is ongoing. Comparisons of measured and computed torque for the UH-1 are shown in Figures 31 and 32; generally favorable results are seen here for the case of zero collective pitch at advance ratios 0.51 and 0.75.

An additional sample of UH-1 correlation results to date is presented in Figures 33 and 34, which illustrate the correlation of measured and predicted H-force. It should be noted at this point that the UH-1 results presented here included a modification to the drag coefficent tables that increased sectional c_d inboard to account for the presence of the doublers out to 0.39R; this modification assumed a bluff body drag characteristic over this region, increasing the sectional drag coefficient (based on chord) to roughly 0.12 over this span.

With this simple model in place, very good correlation was observed for the advance ratio 0.51 case, as shown in Figure 26. However, while correlation was adequate at low shaft angles for advance ratios 0.75 (Figure 27), CHARM missed the observed step-down in H-force at higher shaft angles in this case. It is unclear what physical mechanism would drive such a step-down in these two cases, and investigation of this issue is ongoing. It may be that the experimental rig experiences an unmodeled change in flow separation characteristics in this regime, not easily captured by a simple sectional aerodynamics model.

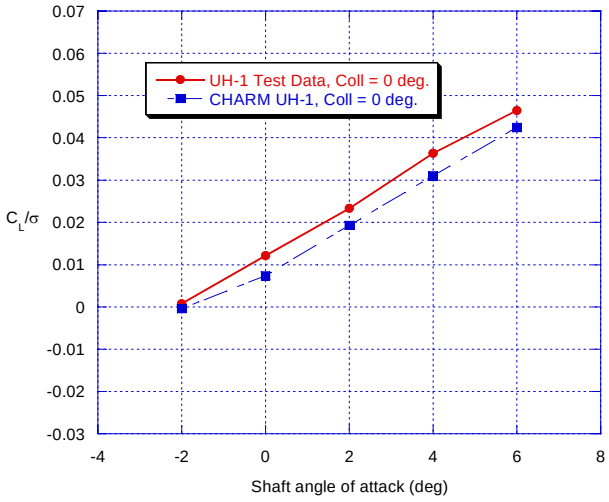

Figure 29: Lift coefficient vs. shaft angle of attack for a modified UH-1 at advance ratio 0.51 and zero deg. collective; predictions using CHARM.

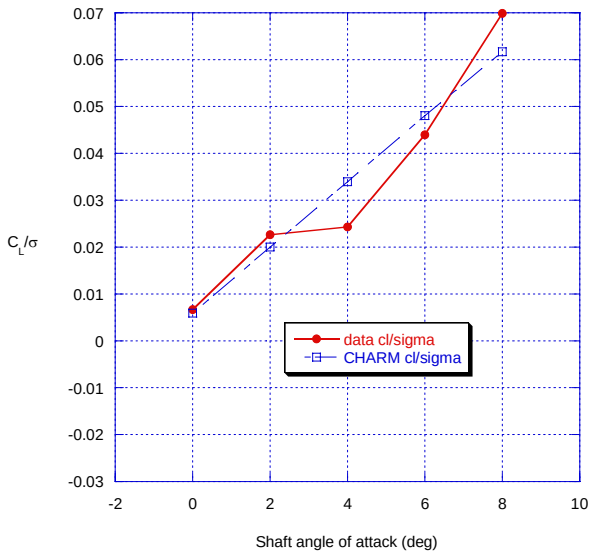

Figure 30: Lift coefficient vs. shaft angle of attack for a modified UH-1 at advance ratio 0.75 and zero deg. collective; predictions using CHARM.

A final correlation study entailed comparison of computed results to the high advance ratio cases discussed in the prior section. In particular, comparison of predicted thrust and torque behavior for Runs 10 and 14 of the final wind tunnel entry are shown in Figures 35 and 36, respectively. As is evident from Figure 35, predictions of lift are generally good for advance ratios

up to 1.0, while predictions of rotor torque are high, as shown in Figure 36. Investigation of the possible role of Reynolds number effects in this overprediction of torque is ongoing.

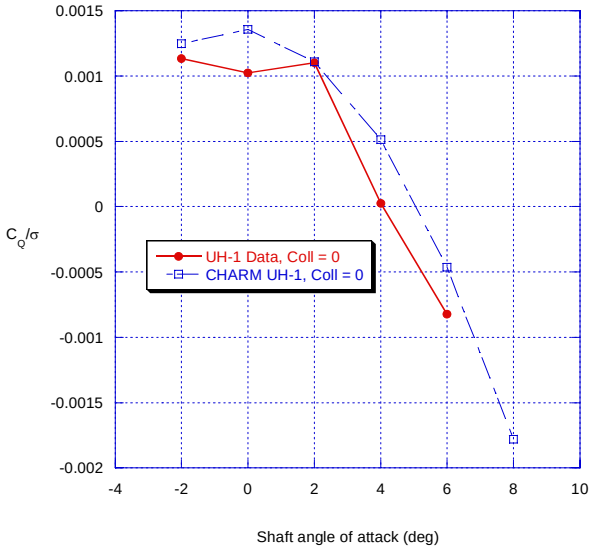

Figure 31: Torque coefficient vs. shaft angle of attack for a modified UH-1 at advance ratio 0.51 at zero collective pitch.

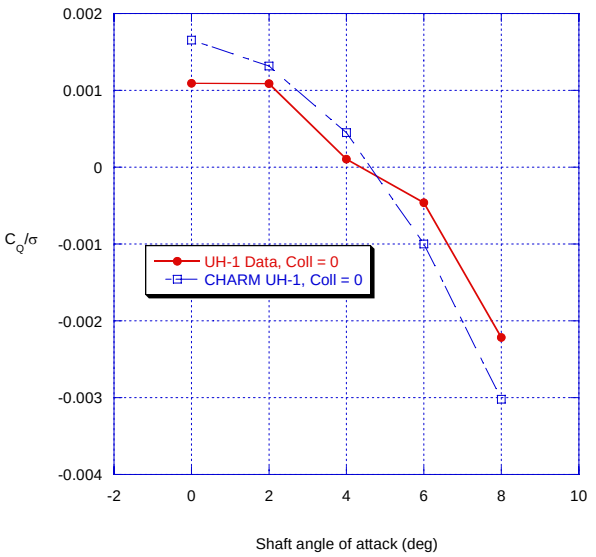

Figure 32: Torque coefficient vs. shaft angle of attack for a modified UH-1 at advance ratio 0.75 at zero collective pitch.

SUMMARY

This paper describes recent activity that has built on and extended earlier milestones in the investigation of high advance ratio aerodynamics, including:

- execution of additional model scale high advance ratio tests at conditions representative of advanced autorotative slowed rotor compound systems, with the achievement of rotor operation up to and beyond μ = 2.0;

- development of data sets for average lift, drag, and in-plane force data for these very high advance ratio cases;

- additional study of blade surface flow via tuft visualization for advance ratios above 1.0, showing evidence of the complexity of flows present, particularly in the third and fourth quadrants.

- measurement of powered rotor performance for selected flight conditions up to advance ratio 1.0

Example applications of analysis tools to the prediction of both full scale and model scale rotor forces were alos presented, showing both a considerable predictive capability but also indicating some ongoing limitations, including difficulties in achieving consistently good predictions of torque and in-plane force for the cases studied.

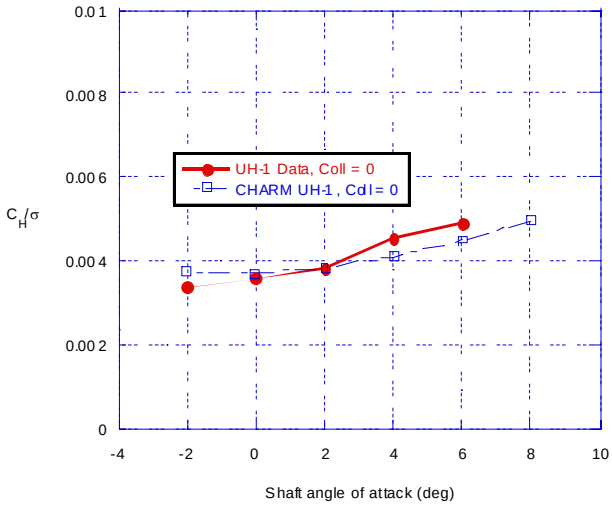

Figure 33: H-force coefficient vs. shaft angle of attack for a modified UH-1 at advance ratio 0.51 at zero collective pitch.

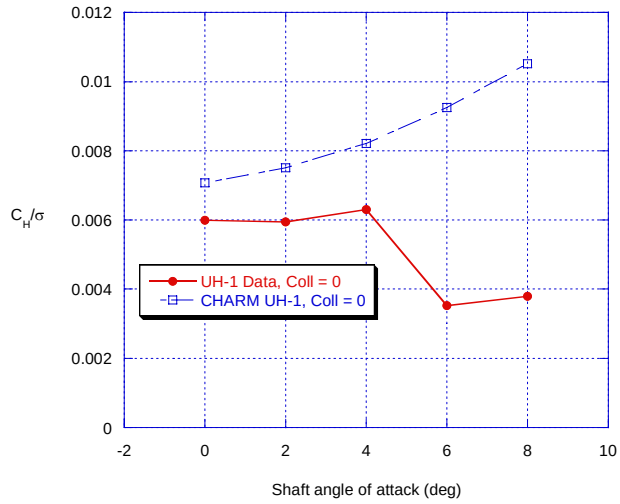

Figure 34: H-force coefficient vs. shaft angle of attack for a modified UH-1 at advance ratio 0.75 at zero collective pitch.

ACKNOWLEDGEMENTS

The research described in this paper was supported by the Rotorcraft Aeromechanics Branch of NASA/Ames Research Center. The technical monitor was Dr.

William Warmbrodt. The authors also wish to acknowledge significant contributions of project collaborators from Georgia Institute of Technology: Profs. Marilyn Smith and Olivier Bauchau and Messrs. Jean de Montaudouin and Seundo Heo.

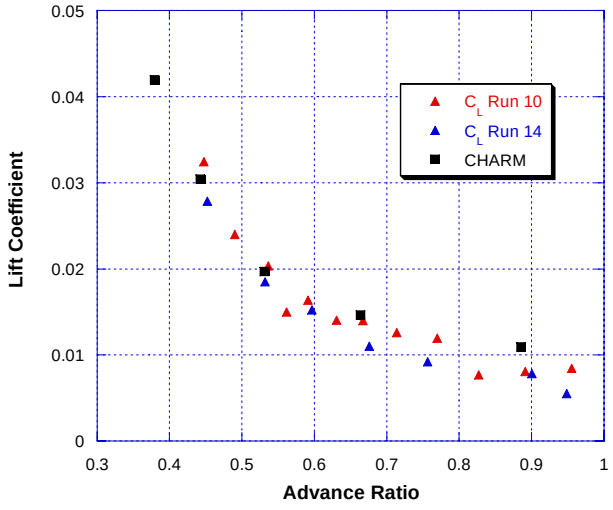

Figure 35: Rotor lift coefficient at fixed tunnel speed of 60 fps; RPM sweep at fixed collective of +3 deg. and fixed shaft angle of -4 deg (Runs 10 and 14), compared to CHARM predictions.

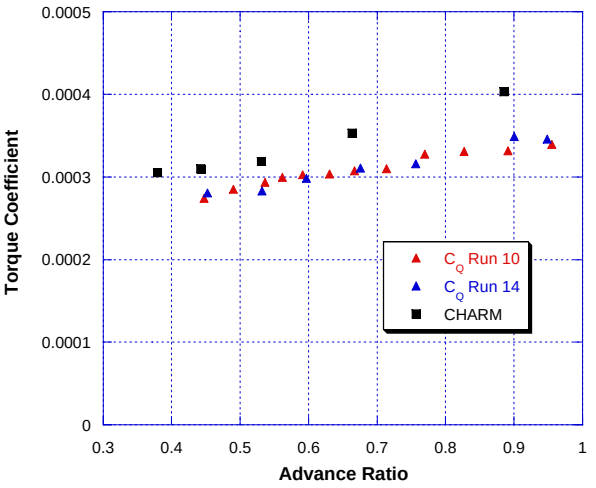

Figure 36: Rotor torque coefficient at fixed tunnel speed of 60 fps; RPM sweep at fixed collective of +3 deg. and fixed shaft angle of -4 deg (Runs 10 and 14), compared to CHARM predictions.

REFERENCES

[1] Wheatley, J. and Hood, M. "Full-Scale Wind-Tunnel Tests of a PCA-2 Autogiro Rotor," NACA TR 515, 1936.

[2] Jenkins Jr., J.L., Sweet, G.E., and Winston, M.M. "Wind-Tunnel Measurements on a Lifting Rotor at High Thrust Coefficients and High Tip-Speed Ratios," NASA-TN-D-2462, Sept. 1964.

[3] Jenkins Jr., J. L. "Wind Tunnel Investigation of a Lifting Rotor Operating at Tip-Speed Ratios from 0.65 to 1.45," NASA-TN-D-2628, Feb. 1965.

[4] McCloud III, J.L., et al. "An Investigation of Full-Scale Helicopter Rotors at High Advance Ratios and Advancing Tip Mach Numbers," NASA-TN-D-4632, July 1968.

[5] Harris, F.D. "An Overview of Autogyros and the McDonnell XV-1," NASA/CR-2003-212799, 2003.

[6] Groen, J. "Groen Brothers Aviation: Autogiros in the 21st Century", AIAA Paper 2003-2519, July 2003.

[7] Carter, J. "Extreme Mu Rotor", U.S. Patent 6986642 2003.

[8] Harris, F.D. "Rotor Performance at High Advance Ratio: Theory vs. Test", NASA CR-2008-215370, 2008.

[9] Bagai, A. "Aerodynamic Design of the X2 Technology Demonstrator™ Main Rotor Blade", Proceedings American Helicopter Society 64th Annual Forum, May 2008.

[10] Quackenbush, T.R. and Wachspress, D.A. "Measurement and Analysis of High Advance Ratio Rotor Performance," Proc. 64th Annual Forum of the AHS, May 2008.

[11] Quackenbush, T.R. et al. "Experimental and Analytical Studies of Lifting Rotor Performance at High Advance Ratios", Proc. AHS Aeromechanics Specialists' Conf., January 2010.

[12] Smith, M.J, et al. "Reverse and Cross-Flow Aerodynamics for High Advance Ratio Flight", Proceedings of the 35th European Rotorcraft Forum, Hamburg, Germany, Sept. 2009.

[13] DeMontaudouin, J., Heo, S., Smith, M.J., and Bauchau, O. "Aerodynamic and Aeroelastic Analysis of Rotors at High Advance Ratios", Proceedings of the 36th European Rotorcraft Forum, Paris, France, Sept. 2010.

[14] Warwick, G. "Groen Brothers Starts work on High-speed VTOL Heliplane for DARPA" Flight International. Vol. 168, no. 5015, pp. 4. 13-19 Dec. 2005

[15] Johnson, W. Helicopter Theory, Princeton University Press, Princeton, NJ, 1980.

[16] Wachspress, D.A., et al. "First-Principles, Free-Vortex Wake Model for Helicopters and Tiltrotors," AHS 59th Annual Forum, Phoenix, AZ, May 2003.

[17] Charles, B.D. and Tanner, H. "Wind Tunnel Investigation of Semirigid Full-Scale Rotors Operating at High Advance Ratio," USAAVLABS-TR-69-2, June 1969.